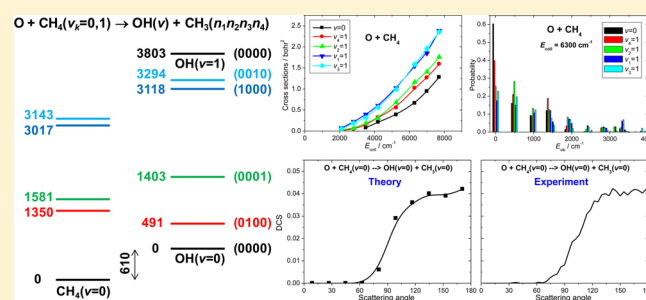


Quasiclassical Trajectory Studies of the $O(^3P) + CX_4(v_k = 0, 1) \rightarrow OX(v) + CX_3(n_1n_2n_3n_4)$ [$X = H$ and D] Reactions on an Ab Initio Potential Energy SurfaceGábor Czakó,^{*,†} Rui Liu,[‡] Minghui Yang,[‡] Joel M. Bowman,[§] and Hua Guo^{||}[†]Laboratory of Molecular Structure and Dynamics, Institute of Chemistry, Eötvös University, H-1518, Budapest 112, P.O. Box 32, Hungary[‡]Key Laboratory of Magnetic Resonance in Biological Systems, State Key Laboratory of Magnetic Resonance and Atomic and Molecular Physics, Wuhan Centre for Magnetic Resonance, Wuhan Institute of Physics and Mathematics, Chinese Academy of Sciences, Wuhan 430071, People's Republic of China[§]Cherry L. Emerson Center for Scientific Computation and Department of Chemistry, Emory University, Atlanta, Georgia 30322, United States^{||}Department of Chemistry and Chemical Biology, University of New Mexico, Albuquerque, New Mexico 87131, United States

S Supporting Information

ABSTRACT: We report quasiclassical trajectory calculations of the integral and differential cross sections and the mode-specific product state distributions for the “central-barrier” $O(^3P) + CH_4/CD_4(v_k = 0, 1)$ [$k = 1, 2, 3, 4$] reactions using a full-dimensional ab initio potential energy surface. The mode-specific vibrational distributions for the polyatomic methyl products are obtained by doing a normal-mode analysis in the Eckart frame, followed by standard histogram binning (HB) and energy-based Gaussian binning (1GB). The reactant bending excitations slightly enhance the reactivity, whereas stretching excitations activate the reaction more efficiently.

None of the reactant vibrational excitations is as efficient as an equivalent amount of translational energy to promote the reactions. The excitation functions without product zero-point energy (ZPE) constraint are in good agreement with previous 8-dimensional quantum mechanical (QM) results for the ground-state and stretching-excited $O + CH_4$ reactions, whereas for the bending-excited reactions the soft ZPE constraint, which is applied to the sum of the product vibrational energies, provides better agreement with the QM cross sections. All angular distributions show the dominance of backward scattering indicating a direct rebound mechanism, in agreement with experiment. The title reactions produce mainly $OH/OD(v = 0)$ products for all the initial states. HB significantly overestimates the populations of $OH/OD(v = 1)$, especially in the energetic threshold regions, whereas 1GB provides physically correct results. The CH_3/CD_3 vibrational distributions show dominant populations for ground ($v = 0$), umbrella-excited ($v_2 = 1, 2$), in-plane-bending-excited ($v_4 = 1$), and $v_2 + v_4$ methyl product states. Neither translational energy nor reactant vibrational excitation transfers significantly into product vibrations.



■ INTRODUCTION

Investigations of the state-to-state dynamics of polyatomic reactions allow tracking of the energy flow along the reaction path, thereby providing insight into the mechanistic details of chemical reactions.¹ Recent experiments are able to measure state-to-state integral and differential cross sections of polyatomic reactions by preparing specific rovibrational states of the reactants and probing various rovibrational states of the products.^{1–5} For polyatomic systems the rigorous computation of these state-to-state data is challenging, because of the high dimensionality of the potential energy surfaces (PESs) and the enormous computational costs of the full-dimensional quantum dynamics approaches. For reactions involving six atoms one can develop chemically accurate full-dimensional PESs,^{6–9} but the quantum computation of the state-to-state cross sections in full

dimensions is still not feasible at present. Therefore, reduced-dimensional quantum methods or full-dimensional quasiclassical trajectory (QCT) calculations are employed to study the dynamics of polyatomic reactions. In both theoretical approaches it is straightforward to investigate the initial-state-specific dynamics; however, the assignment of approximate vibrational quantum numbers to polyatomic products is challenging in QCT. Recently, several QCT product analysis methods were developed to assign normal-mode quantum numbers for polyatomic molecules.^{10–12} Furthermore, two of us¹¹ proposed an efficient technique for applying the so-called

Received: April 17, 2013

Revised: May 27, 2013

Published: June 28, 2013

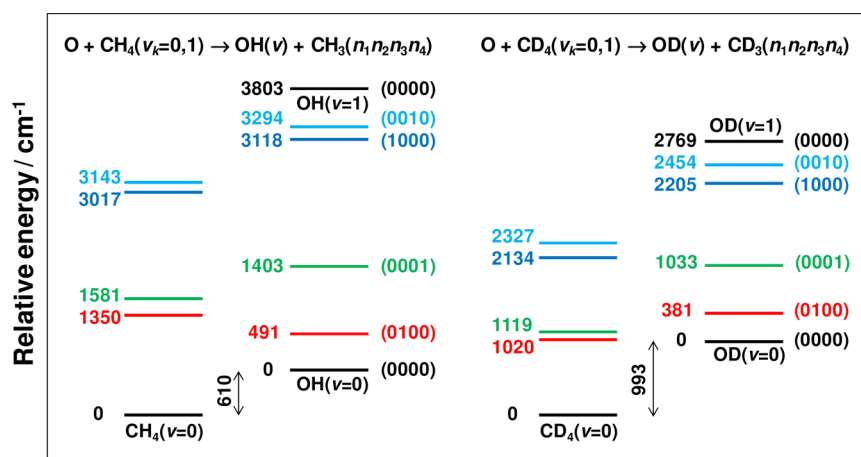


Figure 1. Energetics of the $\text{O}({}^3\text{P}) + \text{CH}_4/\text{CD}_4(v_k = 0, 1)$ [$k = 1, 2, 3, 4$] reactions showing the initial and final fundamental harmonic vibrational states corresponding to the CB PES.⁸

Gaussian Binning (GB)^{13,11,14} method for polyatomic products, thereby giving small weights to trajectories which provide product internal energies far from the corresponding quantum levels. Therefore, the full-dimensional QCT computation of the state-to-state integral and differential cross sections, state-specific product vibrational distributions, and so forth, for six-atom reactions using the sophisticated GB approach and accurate ab initio PESs has become feasible.

The reaction of methane with ground-state oxygen atom, $\text{O}({}^3\text{P})$, plays an important role in combustion processes and, perhaps more importantly, is a benchmark system to study mode-selective polyatomic reactivity. Following the early experiments on the OH and CH_3 product state distributions,^{15,16} Zhang and Liu⁴ measured the first differential cross sections for the $\text{O}({}^3\text{P}) + \text{methane}$ reaction in 2005. In the past few years crossed molecular beam experiments were carried out for the reactions of $\text{O}({}^3\text{P})$ with ground-state CH_4 ,¹⁷ ground-state and bending-excited CD_4 ,⁴ and ground-state and CH-stretching excited CHD_3 .⁵ The early theoretical studies reported semiempirical direct dynamics¹⁸ or reduced-dimensional quantum^{19–22} and reduced-^{23,24} or full-dimensional²⁵ QCT calculations using semiempirical²⁶ or reduced-dimensional ab initio²³ PESs. The first full-dimensional ab initio PES was reported by Czakó and Bowman (CB) in 2012 based on a permutationally invariant fit of 17 212 accurate energy points obtained by an efficient composite method considering electron correlation up to CCSD(T) and basis set effects up to aug-cc-pVQZ.⁸ QCT calculations on the CB PES showed that CH stretching excitation in the $\text{O} + \text{CHD}_3$ reaction enlarges the reactive cone of acceptance,⁸ thereby enhancing the OH + CD_3 products, in agreement with the previous experimental findings.⁵ In a recent Letter we reported 8-dimensional (8D) quantum and full-dimensional QCT results for the integral cross sections of the $\text{O}({}^3\text{P}) + \text{CH}_4(v_k = 0, 1) \rightarrow \text{OH} + \text{CH}_3$ [$k = 1, 2, 3, 4$] reactions using the CB PES.²⁷ The computed results showed that stretching excitations substantially enhance the reactivity, whereas bending/umbrella excitations have a modest effect on the cross sections.²⁷ Furthermore, theory found that translational energy is more efficient to activate the “central-barrier” $\text{O}({}^3\text{P}) + \text{CH}_4$ reaction than an equivalent amount of vibrational energy.²⁷

In the present paper we report detailed QCT studies of the mode-specific state-to-state dynamics of the $\text{O}({}^3\text{P}) + \text{CH}_4/\text{CD}_4 \rightarrow \text{OH}/\text{OD} + \text{CH}_3/\text{CD}_3$ reactions on the ab initio full-

dimensional CB PES⁸ providing integral and differential cross sections as well as mode-specific product state distributions. In our previous QCT study on $\text{O}({}^3\text{P}) + \text{CH}_4$ the integral cross sections were obtained by considering all the trajectories without zero-point energy (ZPE) constraint or weighting. In the present work we consider various treatments for handling the well-known ZPE issue of the QCT method and compare the cross sections to our previous 8D quantum results. Furthermore, we report the first QCT analysis of mode-specific vibrational distributions for the CH_3 and CD_3 products of the $\text{O}({}^3\text{P}) + \text{CH}_4$ and CD_4 reactions, respectively. For the vibrational distributions we also compare the standard histogram binning (HB) with GB. Finally, the new state-to-state QCT results allow comparison between theory and crossed-beam experiments, thereby providing a critical test for the CB PES and the QCT and binning methods.

■ COMPUTATIONAL DETAILS

Initial Conditions. QCT calculations are performed on the CB PES⁸ for the $\text{O}({}^3\text{P}) + \text{CX}_4(v_k = 0, 1) \rightarrow \text{OX} + \text{CX}_3$ [$k = 1, 2, 3, 4$] reactions, where X is H or D and v_4, v_2, v_1 , and v_3 are the umbrella, bending, symmetric stretching, and asymmetric stretching modes of CH_4/CD_4 , respectively. The energetics of the initial and final vibrational states on the CB PES is shown in Figure 1. Standard normal-mode sampling is employed to prepare the initial quasiclassical vibrational ground ($v = 0$) and mode-specific excited states ($v_k = 1$). In previous studies we computed the harmonic vibrational actions of the reactant $\text{CHD}_3(v_k = 1)$ as a function of time and showed that the CH stretching (Figure 2 of ref 11) and various bending (Figure S1 of ref 28) excitation energies do not significantly leak to the other modes prior to the collision; thus, QCT should be able to describe the mode-specific dynamics of the title reactions, as well. The initial distance between the center of mass of the reactants is $(x^2 + b^2)^{1/2}$, where b is the impact parameter and $x = 10$ bohr. The orientation of CH_4/CD_4 is randomly sampled and b is scanned from 0 to 5 bohr with a step size of 0.5 bohr. The actual maximum b (b_{max}) values are found to increase with collision energy (E_{coll}) between 3.0 and 4.5 bohr for the ground-state and bending-excited CH_4 and in the 3.5–5.0 bohr range for the stretching-excited CH_4 . For CD_4 the corresponding b_{max} values are slightly smaller by about 0.5 bohr. Five thousand trajectories are run at each b ; thus, the total number of trajectories is 55 000 for each E_{coll} . QCT calculations are

carried out at 6 and 8 different collision energies in the ranges 3500–7700 and 2100–7700 cm^{-1} for the $\nu = 0$ and $\nu_k = 1$ reactions, respectively. Thus, the present study considers a total of 4 180 000 trajectories. The trajectories are propagated for a maximum of 20 000 steps (1.45 ps) using an integration step of 0.0726 fs, but most of them finish much faster (within a few hundred fs). We stop the trajectories when the actual maximum interatomic distance is 1 bohr larger than the initial one.

Final Conditions. The integral cross sections are calculated using (a) all the trajectories without ZPE constraint, (b) the soft ZPE constraint, (c) the hard ZPE constraint, (d) the methyl vibrational energy-based ZPE constraint, and (e) Gaussian binning. The soft ZPE constraint discards trajectories if the sum of the vibrational energies of the products is less than the sum of the product ZPEs, the hard constraint discards trajectories if the vibrational energy of either product is less than the corresponding ZPE, and methyl vibrational energy-based ZPE constraint is only applied to the polyatomic product. The Gaussian binning is done using the 1GB strategy^{11,14} as briefly described below. The weight of a trajectory is obtained as the product of the weights of the diatomic and polyatomic products.

Based on our previous work,^{11,29} we perform mode-specific vibrational analysis for the methyl product ($N = 4$ atoms), whose center-of-mass Cartesian coordinates, center-of-mass Cartesian velocities, and masses are denoted as \mathbf{r}_i , \mathbf{v}_i , and m_i ($i = 1, 2, \dots, N$), respectively, as follows.

1. We perform a normal-mode analysis at the equilibrium geometry (denoted as \mathbf{r}_i^{eq} in any orientation in the center of mass frame), which provides $3N - 6$ nonzero harmonic frequencies ω_k and the orthogonal transformation matrix $\mathbf{I} \in \mathcal{R}^{(3N-6) \times 3 \times N}$, which transforms from mass-scaled Cartesian coordinates to normal coordinates.

2. We remove the angular momentum by modifying velocities as

$$\mathbf{v}_i^{\text{nr}} = \mathbf{v}_i - \boldsymbol{\Omega} \times \mathbf{r}_i \quad (1)$$

where $\boldsymbol{\Omega} = \mathbf{I}^{-1}\mathbf{j}$, where \mathbf{I}^{-1} is the inverse of the moment of inertia tensor at \mathbf{r}_i and $\mathbf{j} = \sum_{i=1}^N \mathbf{r}_i \times (m_i \mathbf{v}_i)$.

3. For each trajectory \mathbf{r}_i and \mathbf{v}_i are rotated to the Eckart frame corresponding to reference geometry \mathbf{r}_i^{eq} by solving

$$\sum_{i=1}^N m_i \mathbf{r}_i^{\text{eq}} \times (\mathbf{C}(\theta, \phi, \psi) \mathbf{r}_i - \mathbf{r}_i^{\text{eq}}) = \mathbf{0} \quad (2)$$

The matrix \mathbf{C} which transforms to the Eckart frame is obtained as given in eqs 4–8 of ref 29. The Cartesian coordinates, which exactly satisfy the Eckart conditions, and the corresponding velocities are $\mathbf{C}\mathbf{r}_i$ and $\mathbf{C}\mathbf{v}_i^{\text{nr}}$, respectively.

4. The normal coordinates (Q_k) and momenta (P_k) are obtained as

$$Q_k = \sum_{i=1}^N \sqrt{m_i \mathbf{I}_{ki}} (\mathbf{C}\mathbf{r}_i - \mathbf{r}_i^{\text{eq}}) \quad \text{and} \quad P_k = \sum_{i=1}^N \sqrt{m_i \mathbf{I}_{ki}} \mathbf{C}\mathbf{v}_i^{\text{nr}} \quad (3)$$

$$k = 1, 2, \dots, 3N - 6$$

5. The harmonic vibrational energy and the corresponding action for each normal mode are calculated as

$$E_k = \frac{P_k^2}{2} + \frac{\omega_k^2 Q_k^2}{2} \quad \text{and} \quad n'_k = \frac{E_k}{\omega_k} - \frac{1}{2} \quad (4)$$

$$k = 1, 2, \dots, 3N - 6$$

The integer vibrational quanta are obtained by rounding n'_k to the nearest integer value n_k . Since CH_3 and CD_3 have degenerate vibrational modes we assign polyad quantum numbers for the degenerate modes as follows. Let us consider CH_3 with ω_k of 491, 1403, 1403, 3118, 3294, 3294 cm^{-1} for $k = 1, 2, 3, 4, 5, 6$, respectively. Following the Mulliken convention for labeling the modes, the integer quantum numbers for the out-of-plane bending (umbrella), in-plane bending, symmetric stretching, and asymmetric stretching modes are obtained as $n_2(a'_2) = \text{nint}(n'_1)$, $n_4(e') = \text{nint}(n'_2 + n'_3)$, $n_1(a'_1) = \text{nint}(n'_4)$, and $n_3(e') = \text{nint}(n'_5 + n'_6)$, respectively, where nint denotes the nearest non-negative integer. Hereafter we denote a vibrational state $(n_1 n_2 n_3 n_4)$ as \mathbf{n} .

We use both the standard HB and the 1GB methods to calculate the probabilities of the product vibrational states. Using HB and 1GB, the probability of a particular vibrational state \mathbf{n} is obtained as

$$P_{\text{HB}}(\mathbf{n}) = \frac{N(\mathbf{n})}{N_{\text{traj}}} \quad \text{and} \quad P_{\text{GB}}(\mathbf{n}) = \frac{\sum_{p=1}^{N(\mathbf{n})} G_p(\mathbf{n})}{N_{\text{traj}}} \quad (5)$$

respectively. $N(\mathbf{n})$ is the number of products in state \mathbf{n} from the total number of trajectories N_{traj} and

$$G_p(\mathbf{n}) = \frac{\beta}{\sqrt{\pi}} e^{-\beta^2 \left(\frac{E(\mathbf{n}'_p) - E(\mathbf{n})}{2E(\mathbf{0})} \right)^2} \quad p = 1, 2, \dots, N(\mathbf{n}) \quad (6)$$

where $\beta = 2(\ln 2)^{1/2}/\delta$, δ is the full-width at half-maximum, and $E(\mathbf{0})$ is the harmonic ZPE. In eq 6 $E(\mathbf{n})$ is obtained by using the harmonic energy expression

$$E(\mathbf{n}) = \sum_{k=1}^{3N-6} \omega_k \left(n_k + \frac{1}{2} \right) \quad (7)$$

In ref 29 it was shown that neglect of anharmonicity in eq 7 has virtually no effect on the final results. As also shown in ref 29 it is advantageous to calculate $E(\mathbf{n}'_p)$ exactly in the Cartesian space as

$$E(\mathbf{n}'_p) = \frac{1}{2} \sum_{i=1}^N m_i \mathbf{v}_{i,p}^{\text{nr}} (\mathbf{v}_{i,p}^{\text{nr}})^{\text{T}} + V(\mathbf{r}_{1,p}, \mathbf{r}_{2,p}, \dots, \mathbf{r}_{N,p}) - V(\mathbf{r}_1^{\text{eq}}, \mathbf{r}_2^{\text{eq}}, \dots, \mathbf{r}_N^{\text{eq}}) \quad (8)$$

where $\mathbf{v}_{i,p}^{\text{nr}}$ is the velocity of the p -th product corresponding to zero angular momentum as defined in eq 1 and V is the potential energy of the N -atomic product.

In the case of 1GB of the title reaction, we use eq 6 with eqs 7 and 8 to calculate a weight for each CH_3/CD_3 product and similar expressions, given in eqs 17 and 18 of ref 11, are used to calculate a weight for each OH/OD. In the present study the δ values are 0.15 and 0.10 for OH/OD and CH_3/CD_3 , respectively. The weights used in eq 5 to determine the probability of a vibrational state are obtained as products of the weights of CH_3/CD_3 and OH/OD. Finally, we note that we compute the reaction and final-state probabilities at discrete equidistant b values and the corresponding cross sections are obtained by a b -weighted numerical integration over b from 0 to b_{max} .

RESULTS AND DISCUSSION

Integral Cross Sections. Excitation functions for the $\text{O}(^3\text{P}) + \text{CH}_4(\nu_k = 0, 1)$ and $\text{CD}_4(\nu_k = 0, 1)$ reactions without

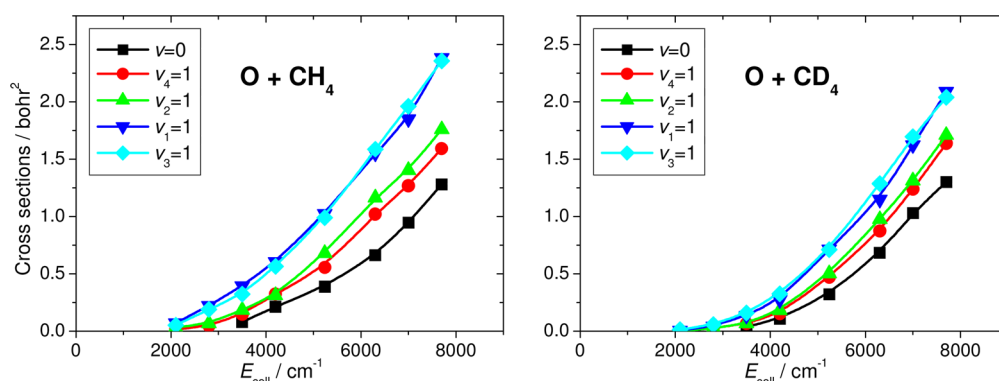


Figure 2. Cross sections as a function of collision energy for the ground-state ($v = 0$), bending-excited (v_4 and v_2), and stretching-excited (v_1 and v_3) $\text{O}(^3\text{P}) + \text{CH}_4/\text{CD}_4(v_k = 0, 1)$ [$k = 1, 2, 3, 4$] reactions obtained by considering all trajectories without ZPE constraint or weighting. The various ZPE-constrained and Gaussian binning results are given in Figures S1 and S2 of the Supporting Information.

ZPE constraint are shown in Figure 2. The various ZPE-constrained and 1GB results are given in Figures S1 and S2 in the Supporting Information. The computed cross sections are very similar for both reactants CH_4 and CD_4 ; thus, the discussion below holds for both reactions. The excitations of the reactant bending modes slightly enhance the reactivity, whereas the excitations of the stretching modes active the reaction more efficiently. The enhancement factors depend on how the ZPE is treated. When all the trajectories are considered the enhancement factors are about 1.2–1.7 for the bending modes and 1.5–2.5 for the stretching modes. The soft and CH_3/CD_3 -based ZPE constraints increase slightly the enhancement factors, whereas the hard ZPE constraint gives significantly larger enhancement, especially for $\text{O} + \text{CH}_4$, where the ZPE issue is expected to be more significant. It is interesting to find that the 1GB method provides similar, just slightly larger, vibrational enhancement factors as the nonconstrained analysis does. These results suggest that the standard ZPE constrained product analysis overestimates the effect of the reactant vibrational excitations, because the ground state reaction is more likely to violate the product ZPEs than the excited-state reactions; therefore, we discard more trajectories for the former. The 1GB method treats both the ground- and excited-state reactions on an equal footing, since small Gaussian weights can be given to both ground- and excited-state products depending on the deviations from the corresponding quantum energy levels. Therefore, the 1GB vibrational enhancement factors should be more realistic than the ZPE constrained ones.

The ZPE constraint obviously decreases the absolute cross sections. For the $\text{O} + \text{CH}_4$ reaction, the (soft, hard, CH_3 -based) ZPE constraints reduce the cross sections, relative to the nonconstrained results, by about (75, 95, 85)%, (35, 80, 55)%, and (15, 65, 40)% for the ground-state, bending-excited, and stretching-excited reactants, respectively. The corresponding numbers for the $\text{O} + \text{CD}_4$ reaction are about (40, 85, 60)%, (20, 70, 40)%, and (10, 55, 30)%, respectively. It is seen that the hard constraint gives significantly smaller cross sections than the soft one. Furthermore, more $\text{O} + \text{CH}_4$ trajectories violate the product ZPEs than $\text{O} + \text{CD}_4$ trajectories, as expected on the basis of the smaller ZPEs of the deuterated isotopologues. In the case of 1GB the computation of realistic absolute cross sections is problematic, due to the normalization issue. As seen in eq 5, we calculate the reaction probabilities as the sum of weights of the reactive trajectories divided by the total number of trajectories. In the denominator one could also

use the sum of weights of all the trajectories; however, we do not attempt to assign weights for nonreactive trajectories. Therefore, we do not compare the absolute 1GB cross sections to the ZPE constrained and nonconstrained ones, although we can note that the present implementation of 1GB gives significantly larger cross sections relative to even the nonconstrained ones.

We recently reported 8-dimensional quantum mechanical (QM) results for the cross sections of the $\text{O} + \text{CH}_4$ reaction using the CB PES.²⁷ In Figure 3 the various ZPE constrained QCT cross sections are compared to the QM results. For the $\text{O} + \text{CH}_4(v = 0)$ reaction the nonconstrained QCT results are in good agreement with the QM data, and the ZPE constrained results, especially the hard ones, substantially underestimate the QM cross sections. For $\text{O} + \text{CH}_4(v_4 = 1)$, the nonconstrained results overestimate the QM ones and the soft and the CH_3 -based results are in reasonably good agreement with the QM cross sections. The hard constraint provides too small cross sections again. The picture is similar for the $\text{O} + \text{CH}_4(v_2 = 1)$ reaction, except that here the soft results almost overlap with the QM ones and the CH_3 -based cross sections are slightly below the QM excitation function. For the stretching-excited reactions the nonconstrained QCT analysis provides good results when comparing to the QM ones. Here the soft ZPE constraint also gives good agreement with QM, especially for the $\text{O} + \text{CH}_4(v_3 = 1)$ reaction, where the soft excitation function agrees even better with the QM one than the nonconstrained results. The hard ZPE constraint seriously underestimates the QM results for the stretching-excited reactions, as well.

Finally, we can compare the shapes and thresholds of the computed and measured excitation functions of the $\text{O} + \text{CH}_4(v = 0)$ reaction. Both theory (QM as well as QCT) and experiment¹⁷ show that the reaction threshold is around 2800 cm^{-1} (8 kcal/mol) and the excitation function displays a concave-up collision energy dependency, whereas the excitation function of the $\text{Cl} + \text{CH}_4(v = 0)$ reaction shows a concave-down behavior, again in agreement between experiment³⁰ and QCT calculations.³¹ We should note that experiment probed the $\text{CH}_3(v = 0)$ products only.³⁰ Nevertheless, as we will discuss later, $\text{CH}_3(v = 0)$ is indeed the dominant product state of the $\text{O} + \text{CH}_4(v = 0)$ reaction.

Differential Cross Sections. Differential cross sections (DCSs) for the $\text{O}(^3\text{P}) + \text{CH}_4(v_k = 0, 1)$ and $\text{CD}_4(v_k = 0, 1)$ reactions are shown in Figure 4. The DCSs are very similar for both the CH_4 and CD_4 reactants. For the ground-state

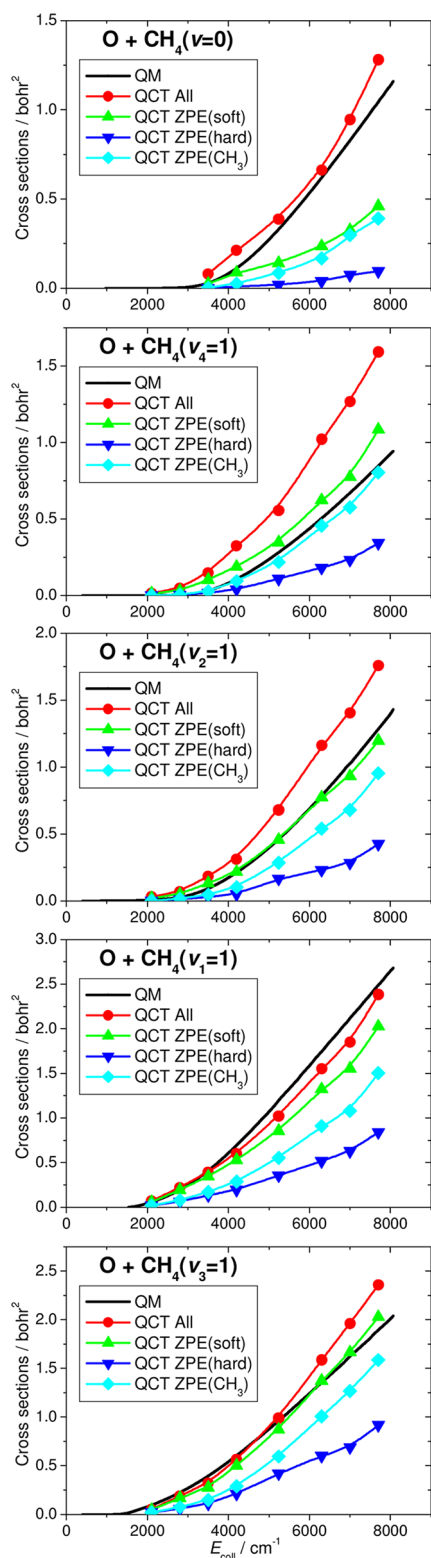


Figure 3. Quantum mechanical (QM) and quasiclassical trajectory (QCT) cross sections as a function of collision energy for the $\text{O}({}^3\text{P}) + \text{CH}_4(\nu_k = 0, 1)$ [$k = 1, 2, 3, 4$] reactions. The 8-dimensional QM results are taken from ref 27 (without including the 2/3 degeneracy factor). The QCT data are obtained by considering (a) all trajectories without ZPE constraint or weighting, (b) soft, (c) hard, and (d) CH_3 -based ZPE constraints, in which trajectories are discarded if (b) the sum of the product vibrational energies is less than the sum of their ZPEs, (c) either product has less vibrational energy than its ZPE, and (d) the CH_3 product has less vibrational energy than its ZPE.

reactions the angular distributions show the dominance of backward scattering in a wide collision energy range of $3500\text{--}7700\text{ cm}^{-1}$. Although slightly more forward scattering can be observed as the collision energy increases, the dominance of the backward directions remains even at the largest collision energies investigated. The picture is different for the analogous $\text{Cl} + \text{CH}_4(\nu = 0)$ reaction, where backward scattering was found at $E_{\text{coll}} \leq 3500\text{ cm}^{-1}$, whereas the DCS clearly showed the dominance of forward scattering at $E_{\text{coll}} = 7000\text{ cm}^{-1}$, in agreement between QCT calculations and experiment.³² These findings indicate that the $\text{O} + \text{CH}_4(\nu = 0)$ reaction occurs with a direct rebound mechanism, whereas the stripping mechanism becomes dominant for the $\text{Cl} + \text{CH}_4(\nu = 0)$ reaction as E_{coll} increases. The maximum impact parameters of 4.5 and 6 bohr of the $\text{O} + \text{CH}_4(\nu = 0)$ and $\text{Cl} + \text{CH}_4(\nu = 0)$ reactions at $E_{\text{coll}} = 7000\text{ cm}^{-1}$, respectively, support the above statement. As Figure 4 also shows, the DCSs do not depend significantly on the initial vibrational states of the reactants, i.e., the dominance of the scattering toward backward directions is seen for the bending- and stretching-excited reactions. The measured DCS of the bending-excited $\text{O} + \text{CD}_4$ reaction was also found to have a similar shape to the DCS of the ground-state reaction,⁴ in agreement with the present QCT results. To the best of our knowledge, DCSs have not been measured for the stretching-excited $\text{O}({}^3\text{P}) + \text{CH}_4$ and CD_4 reactions. It is interesting to note that angular distributions were reported for the CH stretching-excited $\text{O} + \text{CHD}_3$ reaction, where experiment found that the ground-state reaction is clearly backward scattered, whereas significant scattering toward sideways and forward directions appears upon CH stretching excitation.⁵ Recently our QCT study on the CB PES confirmed the experimental finding, i.e., CH stretching excitation enlarges the reactive cone of acceptance in the $\text{O} + \text{CHD}_3$ reaction.⁸ The agreement between the measured and computed DCSs for the CH stretching-excited $\text{O} + \text{CHD}_3$ reaction suggests that the present QCT calculations on the same CB PES provide realistic DCSs for the title reactions. In the view of the stretching effect in $\text{O} + \text{CHD}_3$, it is interesting to find that stretching excitations in $\text{O} + \text{CH}_4$ and CD_4 do not significantly affect the angular distributions.

For the $\text{O}({}^3\text{P}) + \text{CH}_4(\nu = 0) \rightarrow \text{OH}(\nu = 0) + \text{CH}_3(\nu = 0)$ reaction Zhang and Liu reported the experimental angular distributions.¹⁷ To directly compare the present theory to experiment, in Figure 5 we plot the computed DCS ($\text{d}\sigma/\text{d}\cos\theta$) as a function of the scattering angle θ . The QCT results were obtained by using an equidistant binning in θ , and then the cross section for each bin was divided by $\sin\theta$, where θ is the middle of the bin. For the correlated product states, $\text{OH}(\nu = 0)$ and $\text{CH}_3(\nu = 0)$, HB was used, instead of 1GB, which would have required a prohibitively large number of trajectories in order to achieve an acceptable level of statistical accuracy for this final state-specific correlated angular distribution. As Figure 5 shows, the agreement between theory and experiment is excellent, which supports the accuracy of the CB PES and the reliability of the QCT method for this reaction. As also discussed earlier, both theory and experiment show that the angular distributions of the $\text{O} + \text{CH}_4$ reaction are backward-dominant, supporting a direct rebound mechanism.

OH and OD Vibrational Distributions. OH/OD vibrational distributions for the $\text{O}({}^3\text{P}) + \text{CH}_4/\text{CD}_4(\nu_k = 0, 1)$ reactions obtained by HB and 1GB are given in Figure 6. On the CB PES the 0 K enthalpies (based on harmonic ZPEs) of the $\text{O}({}^3\text{P}) + \text{CH}_4$ and CD_4 reactions are 610 and 993 cm^{-1} ,

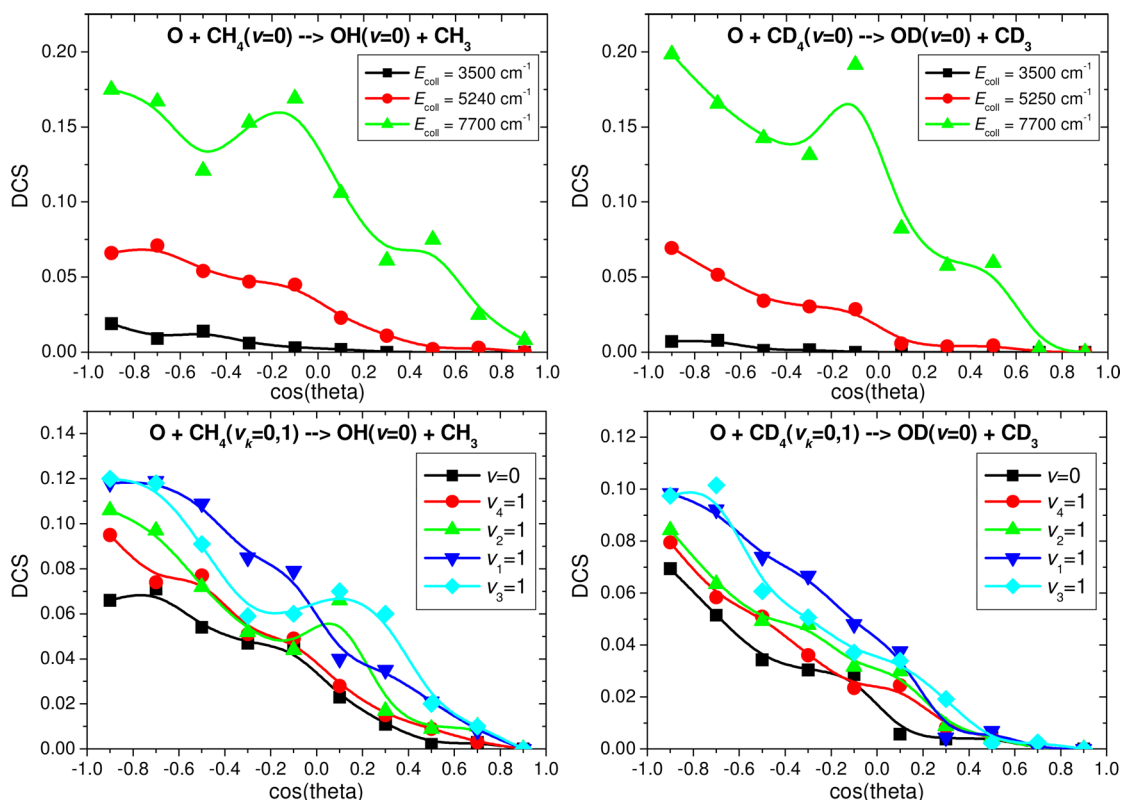


Figure 4. Differential cross sections (DCSs) for the $O(^3P) + CH_4/CD_4(v=0)$ reactions at different collision energies (upper panels) as well as DCSs for the ground-state ($v=0$), bending-excited (v_4 and v_2), and stretching-excited (v_1 and v_3) $O(^3P) + CH_4/CD_4(v_k=0,1)$ [$k=1,2,3,4$] reactions at collision energy of 5250 cm^{-1} (lower panels) obtained by considering all trajectories without ZPE constraint or weighting.

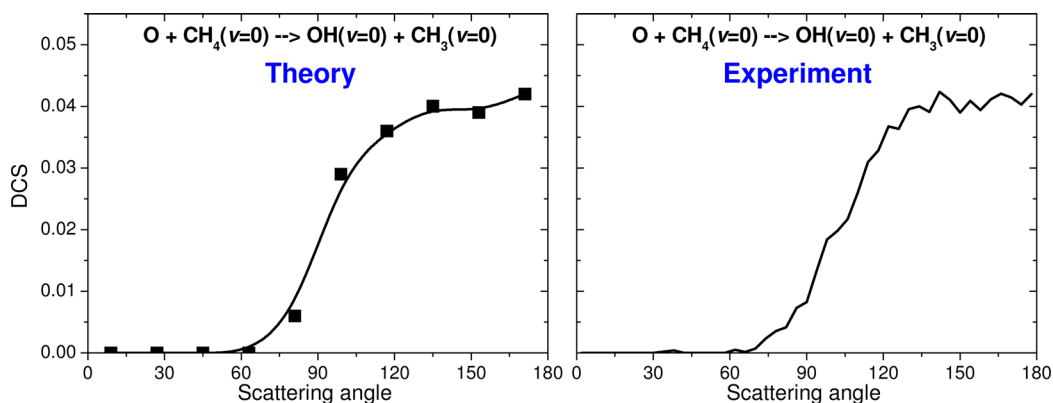


Figure 5. Computed and measured differential cross sections ($d\sigma/d\cos\theta$) for the $O(^3P) + CH_4(v=0) \rightarrow OH(v=0) + CH_3(v=0)$ reaction at collision energies of 15.0 and 14.7 kcal/mol, respectively. The QCT results are obtained by using histogram binning. The experimental data are taken from ref 17.

respectively, and $\omega(OH) = 3803$ and $\omega(OD) = 2769\text{ cm}^{-1}$. Thus, the energetic thresholds of $OH(v=1)$ and $OD(v=1)$ for the $O(^3P) + CH_4/CD_4(v=0)$ reactions are 4413 and 3762 cm^{-1} , respectively (see Figure 1). As Figure 6 shows HB provides significant populations of 35% and 52% for $OH(v=1)$ and $OD(v=1)$, respectively, at $E_{\text{coll}} = 3500\text{ cm}^{-1}$, which is below the thresholds given above. Of course, this is expected, because most of the $OH/OD(v=1)$ products may have less classical vibrational energy than the corresponding quantum energy level and/or the coincident CH_3/CD_3 products may violate ZPE, thereby providing more excitation energy for OH/OD . Both issues are treated by the present 1GB analysis, because we calculate Gaussian weights for both OH/OD and

CH_3/CD_3 and the products of the two weights are used to calculate the OH/OD vibrational distributions. Indeed, Figure 6 shows that the use of 1GB results in 0% fraction of $OH/OD(v=1)$ below the energetic thresholds. Furthermore, 1GB shows that $OH(v=0)$ remains the only product state of the $O + CH_4(v=0)$ reaction over the collision energy range of the present work (E_{coll} up to 7700 cm^{-1}). For $O + CD_4(v=0)$ the $OD(v=1)$ channel opens beyond the threshold energy, but the fraction of $OD(v=1)$ does not exceed 10% even at the largest collision energies. Both HB and 1GB show that bending excitations slightly enhance $OH/OD(v=1)$, whereas stretching excitations have a larger effect on exciting the OH/OD products. However, $OH/OD(v=0)$ remains the major product

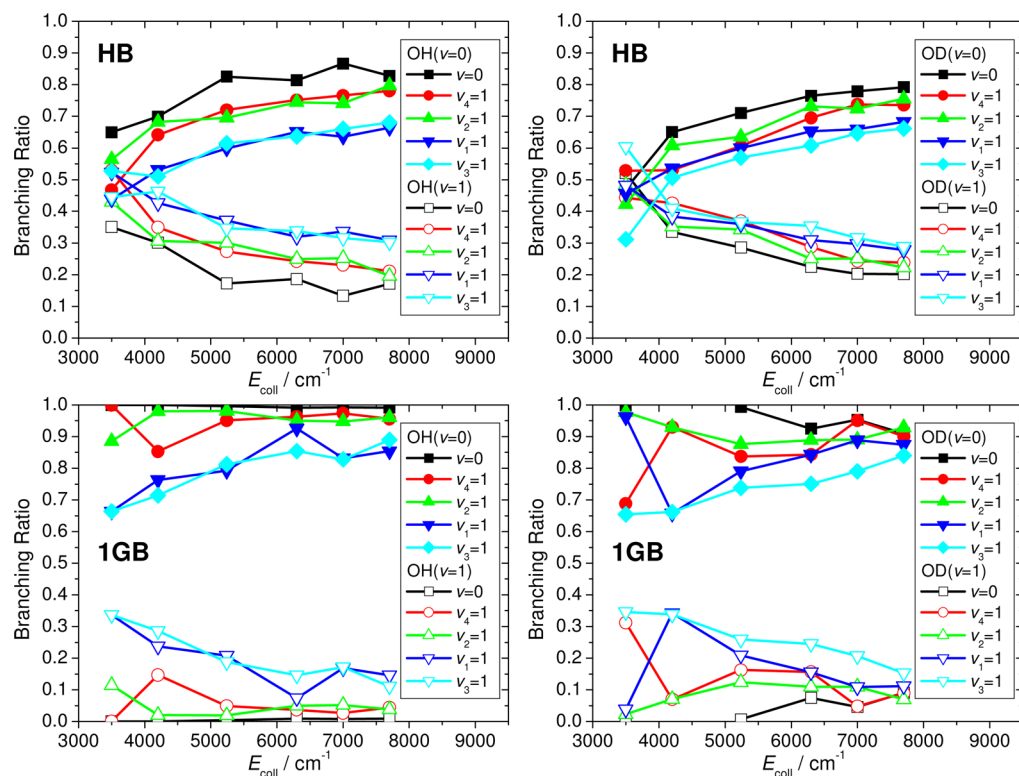


Figure 6. Normalized OH (left) and OD (right) vibrational distributions for the $\text{O}(^3\text{P}) + \text{CH}_4/\text{CD}_4(v_k = 0, 1)$ [$k = 1, 2, 3, 4$] reactions as a function of collision energy. The QCT study employs histogram binning without ZPE constraint (upper panels) and Gaussian binning via the 1GB procedure (lower panels).

state for the stretching-excited reactions, as well. On the basis of the more realistic 1GB results we can conclude that the bending-excited $\text{O} + \text{CH}_4$ reactions produce only about 5% $\text{OH}(v = 1)$, whereas the bending-excited $\text{O} + \text{CD}_4$ reactions give more, about 10%, $\text{OD}(v = 1)$. The stretching-excited reactions produce about 15–30% $\text{OH}/\text{OD}(v = 1)$.

CH_3 and CD_3 Vibrational Distributions. Mode-specific CH_3/CD_3 vibrational distributions for the $\text{O} + \text{CH}_4/\text{CD}_4(v = 0)$ reactions obtained by HB and 1GB at different collision energies are given in Figures 7 and S3. Note that the 1GB vibrational distributions do not change significantly when δ is varied between 0.10 and 0.20 as shown in Figure S4 in the Supporting Information. HB and 1GB provide qualitatively similar vibrational distributions, though notable differences can be observed between the HB and 1GB results. For example, some of the high-energy states around 3000 cm^{-1} have small populations (1–2%) with HB and these states vanish when 1GB is used. Note that neither HB nor 1GB gives nonzero populations for states, which should be closed based on energetic grounds (the maximum available energies for vibration are $E_{\text{coll}} - 610$ and $E_{\text{coll}} - 993 \text{ cm}^{-1}$ for the $\text{O} + \text{CH}_4(v = 0)$ and $\text{CD}_4(v = 0)$ reactions, respectively). This can be contrasted to the $\text{Cl} + \text{CH}_4 \rightarrow \text{H} + \text{CH}_3\text{Cl}$ reaction, where HB provided significant populations for energetically unavailable CH_3Cl states, whereas 1GB gave physically correct results.²⁹ This can be explained by the fact the $\text{Cl} + \text{CH}_4(v = 0)$ reaction produces vibrationally highly excited CH_3Cl products and $\text{CH}_3\text{Cl}(v = 0)$ is just a minor product state, whereas the title reaction produces mainly ground-state CH_3/CD_3 molecules. The 1GB results show that the $\text{O} + \text{CH}_4/\text{CD}_4(v = 0)$ reactions produce no stretching excited CH_3/CD_3 products (HB gives 0–3%). The population of the bending-

excited $\text{CH}_3/\text{CD}_3(v_4 = 1)$ states are around 8–10%, except at the lowest collision energies, where less bending-excitation is seen. As expected, the low-frequency umbrella mode (v_2) is found to be excited by 1–4 quanta, though the dominant product state is usually $v = 0$. Suzuki and Hirota measured the $\text{CH}_3(v_2)$ vibrational distributions for the $\text{O}(^3\text{P}) + \text{CH}_4(v = 0)$ reaction.¹⁶ The observed $\text{CH}_3(v_2)$ vibrational populations monotonically decreased from $v_2 = 0$ to 3 and vanished at $v_2 = 4$, in excellent agreement with the present QCT results (Figure S3, left panel). The finding that $\text{CH}_3(v = 0)$ is the dominant product state of the $\text{O}(^3\text{P}) + \text{CH}_4(v = 0)$ reaction is in agreement with the recent crossed-beam study of Zhang and Liu, as well.¹⁷

The reactant mode-specific CH_3/CD_3 vibrational distributions for the $\text{O} + \text{CH}_4/\text{CD}_4(v_k = 0, 1)$ reactions obtained by 1GB at different collision energies are given in Figure 8 (showing all the product states) and Figure 9 (showing the pure umbrella states only, i.e., $v_2 = 0, 1, 2, \dots$). Considering the available energies of about 10000 cm^{-1} and 9000 cm^{-1} for the stretching-excited $\text{O} + \text{CH}_4(v_{1/3} = 1)$ and $\text{CD}_4(v_{1/3} = 1)$ reactions at $E_{\text{coll}} = 7700 \text{ cm}^{-1}$, respectively, the CH_3/CD_3 vibrational distributions are cold, because the populations tend to vanish at vibrational energies of about 3500 cm^{-1} . For $\text{O} + \text{CH}_4$ the reactant $v_1 = 1$ excitation gives about 2–5% $\text{CH}_3(v_1 = 1)$ and 1–6% $\text{CH}_3(v_3 = 1)$, whereas $\text{O} + \text{CH}_4(v_3 = 1)$ produces about 0–2% $\text{CH}_3(v_1 = 1)$ and 3–8% $\text{CH}_3(v_3 = 1)$. For $\text{O} + \text{CD}_4$ the population of the stretching-excited CD_3 is even less, i.e., 0–1% $\text{CD}_3(v_1 = 1)$ and 0–2% $\text{CD}_3(v_3 = 1)$ for $\text{O} + \text{CD}_4(v_1 = 1)$ and 0–2% $\text{CD}_3(v_1 = 1)$ and 0–3% $\text{CD}_3(v_3 = 1)$ for $\text{O} + \text{CD}_4(v_3 = 1)$. As discussed earlier, the stretching-excited reactions give mostly ground state OH/OD products; thus, reactant stretching excitations transfer mainly into relative

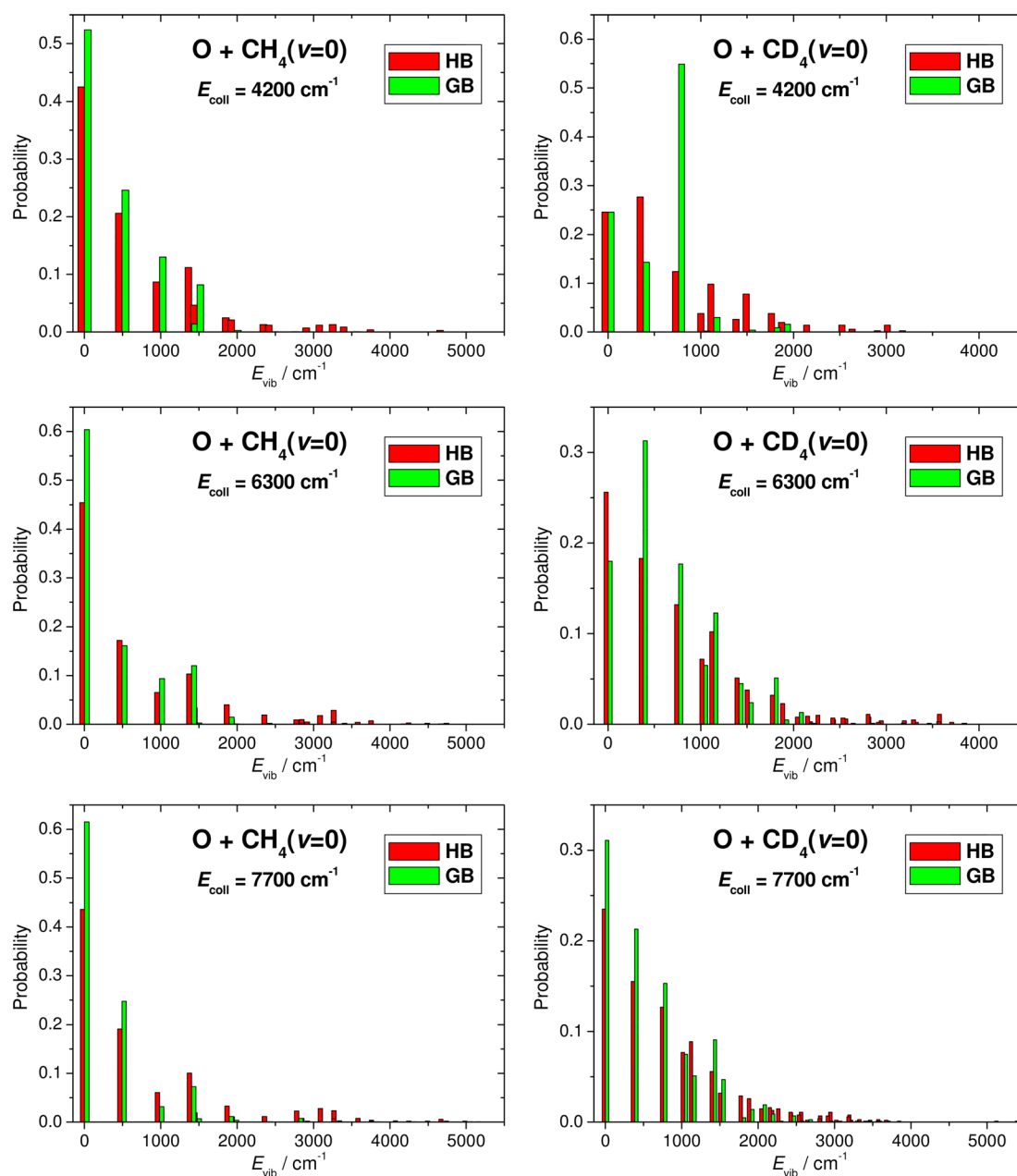


Figure 7. Normalized mode-specific CH_3 (left) and CD_3 (right) vibrational distributions (showing all the product states) for the $\text{O}(^3\text{P}) + \text{CH}_4/\text{CD}_4(\nu = 0)$ reactions at different collision energies obtained by histogram binning (HB) and Gaussian binning via the IGB procedure.

translational energy of the products. For the $\text{O} + \text{CD}_4$ reaction a recent experiment found that bending-excited $\text{O} + \text{CD}_4$ produces less umbrella-excited CD_3 than that from $\text{O} + \text{CD}_4(\nu = 0)$.⁴ Note that in the experiment bending-excitation means the average of $\nu_4 = 1$ and $\nu_2 = 1$. Experimentally only the $\nu_2 = 1$ and 2 excited states of CD_3 were probed. For these excited states the present theory agrees with experiment that the populations of $\text{CD}_3(\nu_2 = 1, 2)$ are less from $\text{O} + \text{CD}_4(\nu_{4/2} = 1)$ than those from $\text{O} + \text{CD}_4(\nu = 0)$ (see Figure 9, and consider the average population of the reactions $\nu_4 = 1$ and $\nu_2 = 1$). However, the QCT results show that the bending-excited $\text{O} + \text{CD}_4(\nu_{4/2} = 1)$ reactions produce larger populations for some of the $\text{CD}_3(\nu_2 > 2)$ states than those from $\text{O} + \text{CD}_4(\nu = 0)$. Overall, the QCT results agree with experiment that bending excitation of CD_4 does not enhance the umbrella-excited CD_3 products. On the other hand, the reactant bending excitation

enhances some of the combination bands of the umbrella (ν_2) and in-plane bending (ν_4) modes, as shown in Figure 8. For the umbrella-excited $\text{O} + \text{CH}_4(\nu_4 = 1)$ reaction the $\text{CH}_3(\nu_2)$ vibrational distributions were computed using a rotating bond umbrella (RBU) quantum model and utilizing a semiempirical PES.¹⁹ The QCT calculations show that at $E_{\text{coll}} = 6300$ and 7700 cm^{-1} the dominant product state of $\text{O} + \text{CH}_4(\nu_4 = 1)$ is $\text{CH}_3(\nu = 0)$, which seems to be in agreement with the RBU quantum results based on the data reported up to about $E_{\text{coll}} = 5400 \text{ cm}^{-1}$. At $E_{\text{coll}} = 4200 \text{ cm}^{-1}$, the RBU study found that $\text{CH}_3(\nu_2 = 1)$ and $\text{CH}_3(\nu_2 = 2)$ are the dominant product states and even $\text{CH}_3(\nu_2 = 3)$ has larger population than $\text{CH}_3(\nu = 0)$.¹⁹ Figure 9, however, shows that the present QCT results predict substantial populations for $\text{CH}_3(\nu = 0)$ and $\text{CH}_3(\nu_2 = 1)$ and negligible $\text{CH}_3(\nu_2 = 2)$ and $\text{CH}_3(\nu_2 = 3)$ at $E_{\text{coll}} = 4200 \text{ cm}^{-1}$.

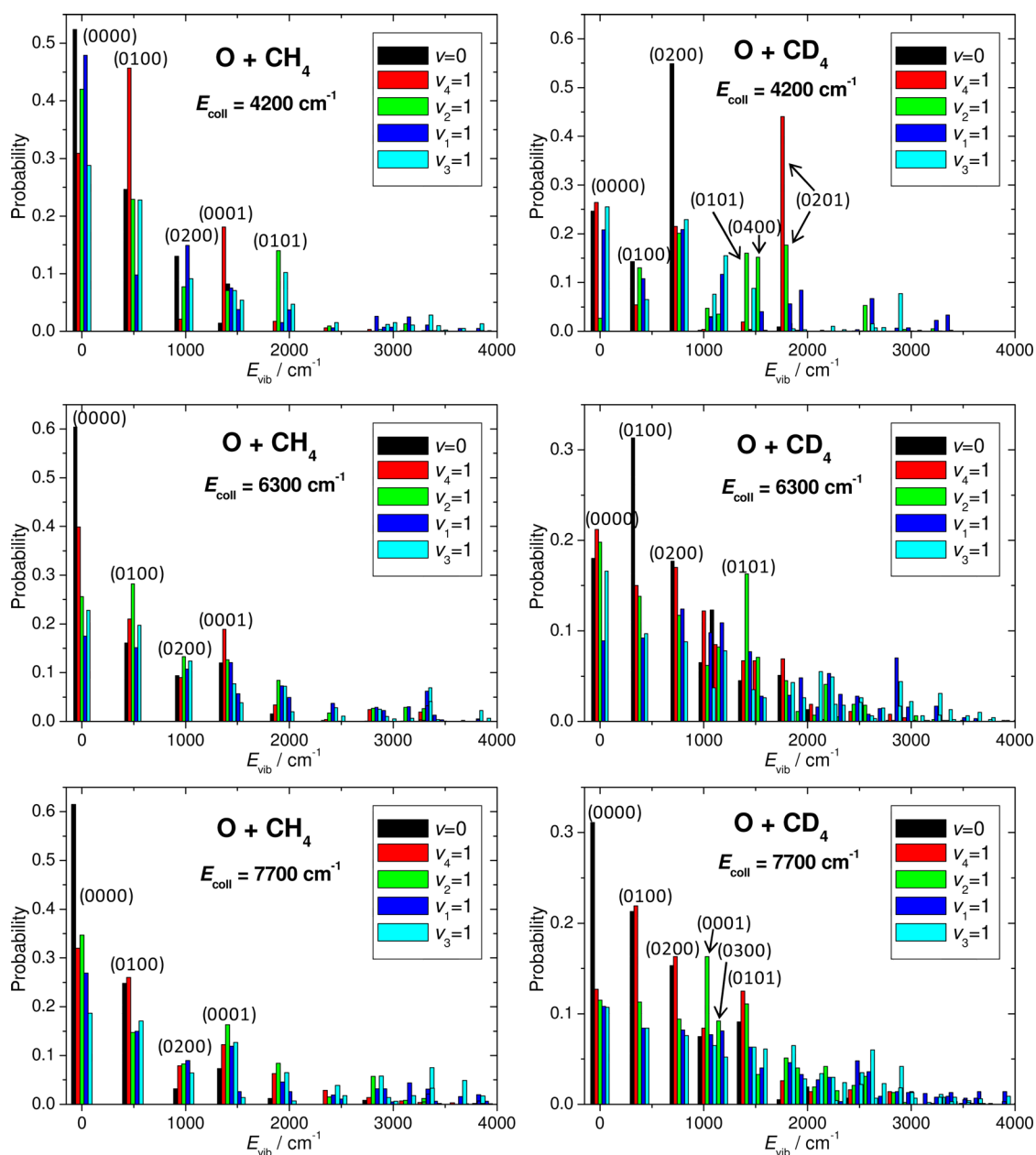


Figure 8. Normalized mode-specific CH_3 (left) and CD_3 (right) vibrational distributions (showing all the product states) for the $\text{O}(^3\text{P}) + \text{CH}_4/\text{CD}_4(v_k = 0, 1)$ [$k = 1, 2, 3, 4$] reactions at different collision energies obtained by Gaussian binning via the 1GB procedure. The harmonic frequencies ($\omega_1, \omega_2, \omega_3, \omega_4$) are (3118, 491, 3294, 1403) cm^{-1} and (2205, 381, 2454, 1033) cm^{-1} for CH_3 and CD_3 , respectively.

To the best of our knowledge, experimental data have not been reported for the bending-excited $\text{O} + \text{CH}_4$ reaction.

SUMMARY AND CONCLUSIONS

We have performed a detailed QCT study for the mode-specific dynamics of the $\text{O}(^3\text{P}) + \text{CH}_4$ and CD_4 reactions using a full-dimensional ab initio PES. Normal mode analysis was done for the CH_3 and CD_3 products after an exact transformation to the Eckart frame. The mode-specific vibrational distributions were computed by using standard histogram binning and Gaussian binning (1GB), where the weights are obtained based on the total vibrational energy of the products. It is important to note that even if 1GB means one Gaussian weight for each product regardless the number of vibrational modes, the present study considers the product of two Gaussians obtained for OH/OD

and CH_3/CD_3 and the advantage of 1GB is taken for one of the two weights corresponding to polyatomic product. This way we can ensure that 1GB handles the usual ZPE issue of the QCT method. The results of the QCT analysis can be summarized as follows.

- (1) The reactant bending (both umbrella and bending) excitations slightly enhance the reactivity and the stretching (both symmetric and asymmetric) excitations have a more substantial effect on the reaction. However, neither bending nor stretching excitation is as efficient as translational energy to activate the “central-barrier” $\text{O} + \text{CH}_4$ and CD_4 reactions. These findings are qualitatively similar with and without ZPE constraint and with and without Gaussian binning.

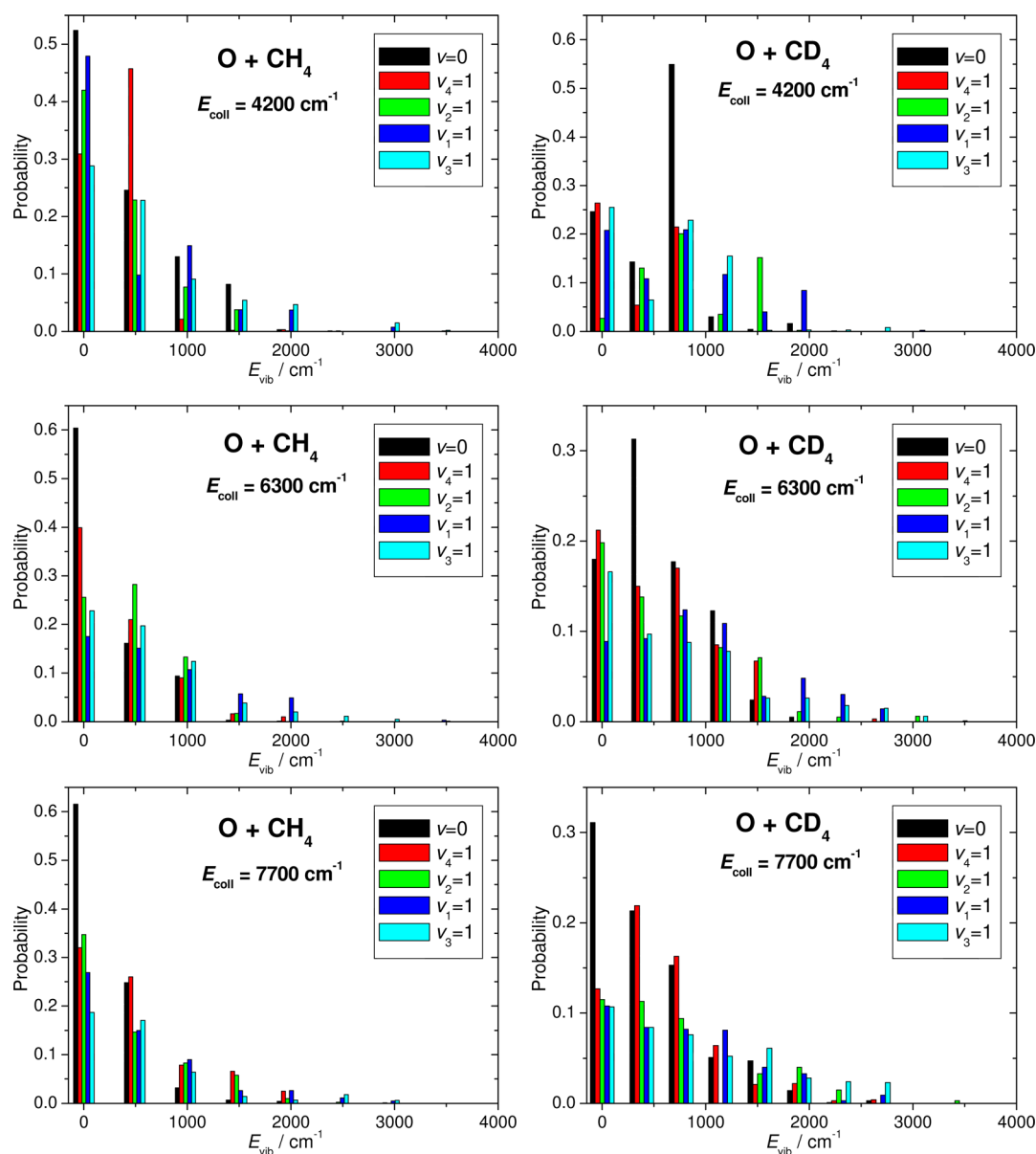


Figure 9. Populations of the umbrella mode (ν_2) excited CH_3 (left) and CD_3 (right) products for the $\text{O}(^3\text{P}) + \text{CH}_4/\text{CD}_4$ ($\nu_k = 0, 1$) [$k = 1, 2, 3, 4$] reactions at different collision energies obtained by Gaussian binning via the IGB procedure. The probabilities are normalized over all the product states, whereas here only the $(0n_200)$ states are shown.

- (2) The absolute integral cross sections are sensitive to the various ZPE constraints. For the $\text{O} + \text{CH}_4$ ($\nu = 0$) reaction the nonconstrained QCT results agree well with the 8-dimensional QM results, whereas the ZPE constrained results underestimate the cross sections. For the umbrella/bending-excited $\text{O} + \text{CH}_4$ ($\nu_{4/2} = 1$) reactions the soft ZPE constraint is the best, whereas the nonconstrained results overestimate and the hard ZPE constraint underestimates the QM cross sections. For the stretching-excited $\text{O} + \text{CH}_4$ ($\nu_{1/3} = 1$) reactions both the nonconstrained and soft ZPE constrained QCT cross sections are in good agreement with the corresponding QM results. It is generally true that the hard ZPE constraint seriously underestimates the cross sections; thus, the soft ZPE constrained and/or nonconstrained QCT analysis should be used for cross section calculations.
- (3) The differential cross sections show that the backward scattering is the dominant for all initial vibrational states of CH_4 and CD_4 investigated in this study, suggesting that the title reactions occur with direct rebound mechanism. The collision energy dependence of the angular distributions is not significant, whereas for the $\text{Cl} + \text{CH}_4$ reaction the dominance of backward scattering shifted toward forward directions with increasing collision energy. Direct comparison between the computed and measured angular distributions for $\text{O} + \text{CH}_4$ ($\nu = 0$) \rightarrow $\text{OH}(\nu = 0) + \text{CH}_3(\nu = 0)$ showed the excellent agreement between theory and experiment¹⁷ and confirmed the accuracy of the ab initio PES.
- (4) HB and IGB provide significantly different OH/OD vibrational distributions. HB shows a large fraction for OH/OD ($\nu = 1$) and allows nonzero populations for energetically nonavailable states. The IGB results are realistic and show that OH/OD ($\nu = 0$) is the dominant

product state for the O + CH₄/CD₄ reactions. Slight enhancement of OH/OD($\nu = 1$) is seen upon umbrella/bending excitations of CH₄/CD₄, and somewhat larger effect, 15–30% OH/OD($\nu = 1$), is found for the stretching-excited reactions.

- (5) The computed mode-specific CH₃/CD₃ vibration distributions show that the title reactions usually produce mainly ground-state methyl products, in agreement with crossed-beam experiments.^{4,17} For O + CH₄($\nu = 0$) the QCT results show monotonically decreasing populations for the umbrella states of CH₃(ν_2) from $\nu_2 = 0$ to 4, in excellent agreement with an early experiment.¹⁶ The O + CH₄/CD₄($\nu = 0$) reactions produce virtually no stretching-excited CH₃/CD₃ products and the enhancement of the stretching-excited methyl products is small (only a few percent or less) upon reactant stretching-excitations.

The findings on the mechanism of the title reactions can be summarized as follows. Both the O + CH₄ and O + CD₄ reactions occur at small impact parameters and proceed through direct rebound pathways. Reactant vibrational excitations do not enlarge the reactive cone of acceptance significantly, because the angular distributions show the dominance of backward scattering for all the initial states. This finding can be contrasted to the O + CHD₃ reaction, where CH stretching excitation enlarges the cone of acceptance, thereby shifting the angular distributions toward sideway and forward directions.^{5,8} The reaction enhancement factors upon initial vibrational excitations show that the stretching modes couple with the reaction coordinate stronger than the bending vibrations. The fact that translational energy activates the reaction more efficiently than vibrational energy shows that this central-barrier reaction behaves more like an early barrier reaction. On the other hand, the product vibrational distributions show the dominance of the ground-state products; thus, most of the energy initially deposited into the reaction system transfers into the relative translational motion of the products. Beside the dominant ground-state, umbrella-excited methyl product states have also significant populations, because the tetrahedral reactant has to form a product that has a planar equilibrium structure.

Overall, the present study shows that the dynamics of the O(³P) + methane reaction can be described well by the QCT method using an accurate PES. Of course, the comparison between the QCT and QM cross sections warrants caution, especially for rate calculations. Experimentally, the effects of the reactant stretching excitations may be studied in the future. Theoretically, we plan to perform QM computations for O + CD₄ and improve the high-energy regions of the PES allowing the study of fast O atom collisions, where multiple product channels open.

■ ASSOCIATED CONTENT

■ Supporting Information

ZPE-constrained and 1GB cross sections for the title reactions and additional 1GB methyl vibrational distributions and their dependence on the full-width at half-maximum. This material is available free of charge via the Internet at <http://pubs.acs.org>.

■ AUTHOR INFORMATION

Corresponding Author

*E-mail: czako@chem.elte.hu.

Notes

The authors declare no competing financial interest.

■ ACKNOWLEDGMENTS

G.C. was supported by the Scientific Research Fund of Hungary (OTKA, NK83583) and the Magyar Fellowship of the European Union and Hungary (TÁMOP 4.2.4.A/1-11-1-2012-0001), R.L. and M.Y. by the National Science Foundation of China (Projects 21073229 and 21221064), J.M.B. by the Department of Energy (DE-FG02-97ER14782), and H.G. by the Department of Energy (DE-FG02-05ER15694). We thank Prof. Kopin Liu for providing the experimental data for Figure 5.

■ REFERENCES

- (1) Yan, S.; Wu, Y.-T.; Liu, K. Tracking the Energy Flow Along the Reaction Path. *Proc. Natl. Acad. Sci. U.S.A.* **2008**, *105*, 12667–12672.
- (2) Yan, S.; Wu, Y. T.; Zhang, B.; Yue, X.-F.; Liu, K. Do Vibrational Excitations of CHD₃ Preferentially Promote Reactivity Toward the Chlorine Atom? *Science* **2007**, *316*, 1723–1726.
- (3) Zhang, W.; Kawamata, H.; Liu, K. CH Stretching Excitation in the Early Barrier F + CHD₃ Reaction Inhibits CH Bond Cleavage. *Science* **2009**, *325*, 303–306.
- (4) Zhang, B.; Liu, K. How Active Is the Bend Excitation of Methane in the Reaction with O(³P)? *J. Phys. Chem. A* **2005**, *109*, 6791–6795.
- (5) Wang, F.; Liu, K. Enlarging the Reactive Cone of Acceptance by Exciting the C-H Bond in the O(³P) + CHD₃ Reaction. *Chem. Sci.* **2010**, *1*, 126–133.
- (6) Czako, G.; Shepler, B. C.; Braams, B. J.; Bowman, J. M. Accurate Ab Initio Potential Energy Surface, Dynamics, and Thermochemistry of the F + CH₄ → HF + CH₃ Reaction. *J. Chem. Phys.* **2009**, *130*, 084301.
- (7) Czako, G.; Bowman, J. M. Dynamics of the Reaction of Methane with Chlorine Atom on an Accurate Potential Energy Surface. *Science* **2011**, *334*, 343–346.
- (8) Czako, G.; Bowman, J. M. Dynamics of the O(³P) + CHD₃($\nu_{\text{CH}} = 0, 1$) Reactions on an Accurate Ab Initio Potential Energy Surface. *Proc. Natl. Acad. Sci. U.S.A.* **2012**, *109*, 7997–8001.
- (9) Czako, G. Accurate Ab Initio Potential Energy Surface, Thermochemistry, and Dynamics of the Br(²P, ²P_{3/2}) + CH₄ → HBr + CH₃ Reaction. *J. Chem. Phys.* **2013**, *138*, 134301.
- (10) Corchado, J. C.; Espinosa-García, J. Product Vibrational Distributions in Polyatomic Species Based on Quasiclassical Trajectory Calculations. *Phys. Chem. Chem. Phys.* **2009**, *11*, 10157–10164.
- (11) Czako, G.; Bowman, J. M. Quasiclassical Trajectory Calculations of Correlated Product Distributions for the F + CHD₃($\nu_1 = 0, 1$) Reactions Using an Ab Initio Potential Energy Surface. *J. Chem. Phys.* **2009**, *131*, 244302.
- (12) Greaves, S. J.; Rose, R. A.; Abou-Chahine, F.; Glowacki, D. R.; Troya, D.; Orr-Ewing, A. J. Quasi-Classical Trajectory Study of the Dynamics of the Cl + CH₄ → HCl + CH₃ Reaction. *Phys. Chem. Chem. Phys.* **2011**, *13*, 11438–11445.
- (13) Bonnet, L.; Rayez, J. C. Quasiclassical Trajectory Method for Molecular Scattering Processes: Necessity of a Weighted Binning Approach. *Chem. Phys. Lett.* **1997**, *277*, 183–190.
- (14) Bonnet, L.; Espinosa-García, J. The Method of Gaussian Weighted Trajectories. V. On the 1GB Procedure for Polyatomic Processes. *J. Chem. Phys.* **2010**, *133*, 164108.
- (15) Sweeney, G. M.; Watson, A.; McKendrick, K. G. Rotational and Spin-Orbit Effects in the Dynamics of O(³P_i) + Hydrocarbon Reactions. I. Experimental Results. *J. Chem. Phys.* **1997**, *106*, 9172–9181.
- (16) Suzuki, T.; Hirota, E. Vibrational Distribution of CH₃ Produced by the Reaction of O(¹D₂) Atom with CH₄. *J. Chem. Phys.* **1993**, *98*, 2387–2398.
- (17) Zhang, B.; Liu, K. Imaging the Reaction Dynamics of the O(³P) + CH₄ → OH + CH₃ Reaction. *Chem. Asian J.* **2011**, *6*, 3132–3136.

(18) Troya, D.; García-Molina, E. Quasiclassical Trajectory Study of the $O(^3P) + CH_4 \rightarrow OH + CH_3$ Reaction with a Specific Reaction Parameters Semiempirical Hamiltonian. *J. Phys. Chem. A* **2005**, *109*, 3015–3023.

(19) Yu, H.-G.; Nyman, G. Quantum Dynamics of the $O(^3P) + CH_4 \rightarrow OH + CH_3$ Reaction: An Application of the Rotating Bond Umbrella Model and Spectral Transform Subspace Iteration. *J. Chem. Phys.* **2000**, *112*, 238–247.

(20) Palma, J.; Clary, D. C. A Quantum Model Hamiltonian to Treat Reactions of the Type $X + YCZ_3 \rightarrow XY + CZ_3$: Application to $O(^3P) + CH_4 \rightarrow OH + CH_3$. *J. Chem. Phys.* **2000**, *112*, 1859–1867.

(21) Palma, J.; Clary, D. C. Improving Reduced Dimensionality Quantum Reaction Dynamics with a Generalized Transition State. Application to $CH_4 + O(^3P)$. *J. Chem. Phys.* **2001**, *115*, 2188–2197.

(22) Yang, M.; Lee, S.-Y.; Zhang, D. H. Seven-Dimensional Quantum Dynamics Study of the $O(^3P) + CH_4$ Reaction. *J. Chem. Phys.* **2007**, *126*, 064303.

(23) González, M.; Hernando, J.; Millán, J.; Sayós, R. Ab Initio Ground Potential Energy Surface, VTST and QCT Study of the $O(^3P) + CH_4(X^1A_1) \rightarrow OH(X^2\Pi) + CH_3(X^2A_2')$ Reaction. *J. Chem. Phys.* **1999**, *110*, 7326–7338.

(24) Martínez, R.; Enriquez, P. A.; Puyuelo, M. P.; Gonzalez, M. Dynamics of the $O(^3P) + CH_4 \rightarrow OH + CH_3$ Reaction Is Similar to That of a Triatomic Reaction. *J. Phys. Chem. A* **2012**, *116*, 5026–5029.

(25) Troya, D.; Pascual, R. Z.; Schatz, G. C. Theoretical Studies of the $O(^3P) + Methane$ Reaction. *J. Phys. Chem. A* **2003**, *107*, 10497–10506.

(26) Espinosa-García, J.; García-Bernáldez, J. C. Analytical Potential Energy Surface for the $CH_4 + O(^3P) \rightarrow CH_3 + OH$ Reaction. Thermal Rate Constants and Kinetic Isotope Effects. *Phys. Chem. Chem. Phys.* **2000**, *2*, 2345–2351.

(27) Liu, R.; Yang, M.; Czako, G.; Bowman, J. M.; Li, J.; Guo, H. Mode Selectivity for a "Central" Barrier Reaction: Eight-Dimensional Quantum Studies of the $O(^3P) + CH_4 \rightarrow OH + CH_3$ Reaction on an Ab Initio Potential Energy Surface. *J. Phys. Chem. Lett.* **2012**, *3*, 3776–3780.

(28) Czako, G.; Shuai, Q.; Liu, K.; Bowman, J. M. Communication: Experimental and Theoretical Investigations of the Effects of the Reactant Bending Excitations in the $F + CHD_3$ Reaction. *J. Chem. Phys.* **2010**, *133*, 131101.

(29) Czako, G. Gaussian Binning of the Vibrational Distributions for the $Cl + CH_4(v_{4/2} = 0, 1) \rightarrow H + CH_3Cl(n_1n_2n_3n_4n_5n_6)$ Reactions. *J. Phys. Chem. A* **2012**, *116*, 7467–7473.

(30) Zhou, J.; Zhang, B.; Lin, J. J.; Liu, K. Imaging the Isotope Effects in the Ground State Reaction of $Cl + CH_4$ and CD_4 . *Mol. Phys.* **2005**, *103*, 1757–1763.

(31) Czako, G.; Bowman, J. M. Accurate Ab Initio Potential Energy Surface, Thermochemistry, and Dynamics of the $Cl(^2P, ^2P_{3/2}) + CH_4 \rightarrow HCl + CH_3$ and $H + CH_3Cl$ Reactions. *J. Chem. Phys.* **2012**, *136*, 044307.

(32) Zhang, B.; Liu, K.; Czako, G.; Bowman, J. M. Translational Energy Dependence of the $Cl + CH_4(v_b = 0, 1)$ Reactions: A Joint Crossed-Beam and Quasiclassical Trajectory Study. *Mol. Phys.* **2012**, *110*, 1617–1626.